

UKAEA-CCFE-PR(19)22

M.J. Lloyd, R.G. Abernethy, D.A.J. Armstrong, P.A.J.
Bagot, M.P. Moody, E. Martinez, D. Nguyen-Manh

Radiation-Induced Segregation in W-Re: From Kinetic Monte-Carlo Simulations to Experimental Validation

Enquiries about copyright and reproduction should in the first instance be addressed to the
UKAEA
Publications Officer, Culham Science Centre, Building K1/0/83 Abingdon, Oxfordshire,
OX14 3DB, UK. The United Kingdom Atomic Energy Authority is the copyright holder.

Radiation-Induced Segregation in W-Re: From Kinetic Monte-Carlo Simulations to Experimental Validation

M.J. Lloyd, R.G. Abernethy, D.A.J. Armstrong, P.A.J. Bagot, M.P. Moody, E. Martinez, D. Nguyen-Manh

Radiation-Induced Segregation in W-Re: From Kinetic Monte Carlo Simulations to Experimental Validation

Matthew J. Lloyd^{1,2}, Robert G. Abernethy^{1,2}, David E. J. Armstrong¹, Paul A. J. Bagot¹, Michael P. Moody¹, Enrique Martinez³, and Duc Nguyen-Manh^{1,2}

¹ Department of Materials, University of Oxford, Parks Road, Oxford, Oxfordshire, OX13PH, UK

² Culham Centre for Fusion Energy, United Kingdom Atomic Energy Authority, Culham Science Centre, Abingdon, Oxfordshire, OX143DB, UK

³ Theoretical Division, Los Alamos National Laboratory, Los Alamos, New Mexico, USA

Received: date / Revised version: date

Abstract. A viable fusion power station is reliant on the development of plasma facing materials that can withstand the combined effects of high temperature operation and high neutron doses. In this study we focus on W, the most promising candidate material. Re is the primary transmutation product and has been shown to induce embrittlement through cluster formation and precipitation below its predicted solubility limit in W. We investigate the mechanism behind this using a kinetic Monte Carlo model, implemented into Stochastic Parallel Particle Kinetic Simulator (SPPARKS) code and parameterised with a pairwise energy model for both interstitial and vacancy type defects. We also compliment our computational work with atom probe tomography of ion implanted, model W-Re alloys. By introducing point defect sinks into our simulation cell, we observe the formation of Re rich clusters which have a concentration similar to that observed in ion irradiation experiments.

PACS. PACS-key describing text of that key – PACS-key describing text of that key

1 Introduction

The realisation of fusion energy is dependant on the development of high performance materials that can withstand the extreme conditions that they will be subjected to. The plasma facing components of a fusion reactor will experience a combination of high thermal loading (10MWm^{-2} [1]) and an intense flux of both 14 MeV neutrons and high energy He/H ions, meaning they will have to operate at very high temperatures (1300 K). Tungsten is currently the leading candidate material due to its high melting temperature (3695K), good thermal conductivity, resistance to sputtering and low activation under neutron irradiation [2,3]. But at such a high neutron flux, transmutation of W in a fusion reactor is significant, resulting in several at.% Re, Os and Ta over the lifetime of the reactor [4]. Precipitation of Re and Os has been observed well below their solubility limit in W, resulting in embrittlement, hardening, and a reduction in thermal conductivity. In this study we investigate the precipitation of Re in W-Re using a kinetic monte carlo (KMC) algorithm, with a pairwise interaction energy model, parameterised by Density Functional Theory (DFT) .

Transmutation of the W plasma facing components (PFCs) occurs in a reactor through the interaction of the material with 14MeV neutrons produced in the fusion reaction in the reactor core. Neutron absorption and subsequent alpha decays leads to the production of helium. The beta decay of W nuclei that have absorbed a neutron produces Re and Os, whereas Ta is produced by neutron loss (n,2n) reactions in W and subsequent beta decay . At various points in the lifetime of the components, the ratios of these elements will vary [4,5], resulting in a material that has a time dependant composition. After 2 full power years under a DEMO like spectrum, an initially pure W PFC is predicted to develop a concentration of 0.8at.%Re, 0.2at.%Ta and 0.05at.%Os, though at longer exposure times the level of Os is expected to exceed the level of Ta [4]. Spatial inhomogeneities in the neutron flux leads to variation in the level of transmutation at various locations around the reactor [5]. This represents a unique challenge for reactor designers, and an understanding of how precipitation occurs is essential for predicted component lifetimes.

Direct testing of W components with fusion spectrum neutrons is not currently possible as there is no facility capable of producing the combination of high neutron fluxes and high temperatures for sustained periods of time. Instead, heavy ion [6,7], proton [8], and fission spectrum

neutron irradiation campaigns [9–13] are used to simulate neutron damage in tungsten. A. Xu et. al investigated binary W-2Re alloys and ternary W-2Re-1Os/W-2Re-1Ta alloys, ion irradiated using W self ions to 33 dpa, using APT [6,7]. Clear precipitation of Re was seen at 573 and 773 K, with Os acting to suppress the precipitation of Re by preferentially forming small Os rich clusters, 1.9 nm average diameter compared to 3.3 nm in the binary alloy. Though similar in composition to the predicted transmutation levels, A. Xu et. al’s work focused on temperatures lower than the planned operating temperature of tungsten in a reactor. In addition to this, a consensus has not yet been reached on the use of ions to simulate neutron damage.

Several neutron irradiation campaigns have been conducted since the 1990s. Hasegawa et al have carried out irradiations at a range of temperatures and doses at JOYO, HFIR and JMTR, producing a schematic diagram of the damage produced at these conditions [10]. Void and precipitate formation has been shown to be favoured at higher temperatures and doses. Recent work by Hu et al has used HAADF imaging and EDX mapping to study transmutation induced precipitation in more detail [12]. Clear precipitation was observed with Re and Os forming lenticular precipitates and decorating grain boundaries. Os was seen to form in the centre of these clusters and voids were shown to be associated with precipitates. The level of transmutation products present in these samples, particularly the Os content, was higher than is predicted to be present in a fusion reactor. The temperatures used during irradiation were also lower than the operating temperature of W in a reactor (maximum of 800C). Klimenkov et al studied the behaviour of these precipitates in materials with more realistic compositions using samples produced in the Extremat II program [9]. Re was clearly shown to decorate grain boundaries and form small precipitates in the centres of grains. No Os segregation to the grain boundaries was seen in the polycrystalline material but in the single crystal, a small amount of signal from the Os correlated with the Re clusters was seen. Voids detected in this material using Scanning Tunnelling Electron Microscopy (STEM) have been shown to be decorated with Re and Os [13]. The process through which these precipitates form is still not clear, with different mechanisms proposed to explain their formation.

Kinetic Monte Carlo (KMC) simulations of W-Re have shown the importance of the mixed interstitial for precipitation, which unlike the self-interstitial which is confined to 1D motion, is able to move through a series of rotations and translations, to effectively migrate in 3D [14–16]. The increased mobility of the mixed interstitial has been shown to facilitate the nucleation and growth of Re clusters, despite the predicted solid solution [17]. Models such as this rely on a simple Ising-like model, which uses pairwise interactions to construct process rates, such as migration and rotation. The pairwise binding energy of the di-vacancy in W is close to zero, which results in a potential underestimation of the role of vacancies within this model. The use of a cluster expansion Hamiltonian

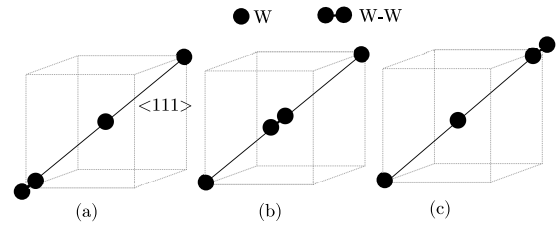


Fig. 1. Schematic diagram of the migration pathway for a self interstitial dumbbell in W, orientated along the 111 direction. Reproduced from [14]

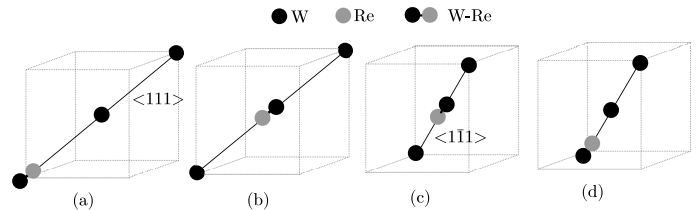


Fig. 2. Schematic diagram showing the migration pathway for the W-Re mixed interstitial dumbbell in W. In the case of the mixed dumbbell, migration occurs through a series of rotation and translation events, which from a to d effectively results in a migration along the 100 direction. Reproduced from [14]

can overcome this problem by considering interactions between 3 or more atoms/defects at once. At high temperatures (stage IV Recovery [3]) vacancies become much more mobile and play a more significant role in microstructural evolution. Monte Carlo (MC) simulations using a cluster expansion (CE) Hamiltonian have predicted the precipitation of Re in W alloys through the formation of small voids, decorated with Re atoms [18].

2 Computational Methodology

The basis of the model presented here is the Monte Carlo technique, which relies on the generation of random numbers to sample a distribution of possible events. For the study of the diffusion of defects, the difference in the energy, $\Delta E_{i \rightarrow j}$, between two states, i and j is used to generate the probability of a particular rate occurring. To construct this change in energy between states, we rely on pairwise energies, obtained using DFT. These pairwise potentials, ε , are summed for the initial and final state to produce a total initial and final energy, according to a broken-bond model.

The change in energy can then be used to calculate the probability of a particular event occurring. In this research we utilise this change in energy in two ways. The first is within a Semi Grand Canonical MC (SGMC) model, in which the equilibrium composition of Re is obtained for a given chemical potential in the solid solution phase. The second uses the energy difference between the saddle point and the minimum of each transition to calculate the rate of a particular event, relying on harmonic transition state theory, facilitating Kinetic MC (KMC) simulations.

The model we present in this study is implemented into the open source Stochastic Parallel Particle Kinetic Simulator (SPPARKS) code. We include 3 types of point defects: vacancies, self-interstitial dumbbells and mixed interstitial dumbbells. We do not currently consider the Re-Re interstitial dumbbell.

2.1 Semi-Grand Canonical Monte Carlo

In the SGMC model, atoms are exchanged from a reservoir, using a probability which is given by the change in energy before and after the swap, $\Delta E_{i \rightarrow j}$. Atoms are selected at random from the box. If a W atom is selected it is swapped to a Re atom and vice versa, with a probability $\prod_{i \rightarrow j}$, given by equation 1, where ΔN_{Re} is the change in the number of Re atoms, $\Delta \mu$ is the change in chemical potential, and T is the temperature.

$$\prod_{i \rightarrow j} = \min \left\{ 1, \exp \left(\frac{-\Delta E_{i \rightarrow j} \pm \Delta \mu \Delta N_{\text{Re}}}{k_B T} \right) \right\} \quad (1)$$

For a fixed temperature and chemical potential, $\Delta \mu$, the concentration of Re within the box is allowed to fluctuate through swaps with the reservoir until the system reaches equilibrium. Inside a miscibility gap where a mixture of phases are present, the change in chemical potential does not determine the composition of the system. The system is therefore not stable within these regions and jumps to a higher concentration. By plotting the change in chemical potential, $\Delta \mu$ against the equilibrium concentration of Re, the miscibility gap is shown as a step in the plot.

By starting simulations with a concentration of defects, the equilibrium configuration of the system with a given chemical potential and temperature can be obtained. Defects are allowed to exchange with atoms, based on a probability given by equation 2, where ΔE_{ij} in this case is the change in energy before and after the jump.

$$\prod_{i \rightarrow j} = \min \left\{ 1, \exp \left(-\frac{\Delta E_{i \rightarrow j}}{k_B T} \right) \right\} \quad (2)$$

Evolving the system with a fixed concentration of defects allows us to study the equilibrium configuration of the defects within the box for a given Re concentration.

2.2 Kinetic Monte Carlo

2.2.1 Defect Migration

The SGMC algorithm can provide insight into the equilibrium configuration of a particular defect and solute concentration, but in order to study the Re clustering/ precipitation kinetics, a KMC model must be used. The KMC model follows harmonic transition state theory (TST), in which the change in energy between states i and j (the initial state and saddle point between initial and final states),

ΔE_{ij} , is used to generate the rate, $\lambda_{i \rightarrow j}$, of a process occurring, by multiplying by the attempt frequency, ν , (which depends on the type of defect, $\nu_V = 6.5 \times 10^{12} \text{Hz}$ for vacancies and $\nu_I = 1.5 \times 10^{12} \text{Hz}$ for interstitials) as shown in equation 3. We use this expression to approximate the rates associated with all defect types within our model (vacancies, self-interstitials and mixed interstitials). Interstitials migrate quickly as the activation energy for their movement and rotation is very low compared to the vacancies, making it closer to kT . TST is valid for events with high activation energies such as the vacancies, but when this barrier is lower (such as for interstitials) the validity of this approach is more questionable due to the increased probability of tunnelling through the barrier.

$$\lambda_{i \rightarrow j} = \nu \cdot \exp \left(-\frac{\Delta E_{i \rightarrow j}}{k_B T} \right) \quad (3)$$

The calculation of the change in energy, ΔE_{ij} , varies for different defects. There are different migration pathways for vacancies, self-interstitials and mixed interstitials. For vacancies we consider the energetics of the defect at the saddle point of the jump between the initial and final states to determine its rate. As shown in figure 4, the energy is constructed using the sum of the pairwise energies, ε , according to the so-called broken-bond model.

$$\Delta E_{i \rightarrow j}^V = \sum_p \varepsilon_{\alpha-p}^{\text{sp}} - \sum_q \varepsilon_{\alpha-q}^{(n)} - \sum_{r \neq \alpha} \varepsilon_{V-r}^{(n)} + \sum \Delta E_{i \rightarrow j}^c \quad (4)$$

The 4 terms which contribute toward this sum on the RHS of equation 4 are, from left to right, the sum on the pairwise interactions at the saddle point, the sum of the pairwise interactions between the atom α in its original position with its neighbours, q , the interaction between the vacancy and its neighbours, r (not including that between the vacancy and the swapping atom α as this has already been counted) and finally the contribution to the change in energy due to the change in the concentration of solute. These sums are carried out to the i th nearest neighbour which in our case is fixed to 2NN.

For the interstitial, the change in energy is not considered at the saddle point. The calculation is simply approximated at the initial and final positions. In the case of the self interstitial, the change in energy is given by equation 5 where $E_m^{\text{SIA}} = 0.003 \text{eV}$ [17]. The self interstitial migrates along a set $\langle 111 \rangle$ direction, chosen at random when it is inserted into the simulation cell. In addition to its migration, the SIA has a probability of rotating to a new $\langle 111 \rangle$ direction with a probability given by equation 3 where the change in energy is a fixed activation energy for rotation, $E_R^{\text{SIA}} = 0.43$ [17].

$$\Delta E_{i \rightarrow j} = E_m^{\text{SIA}} + \sum_p \varepsilon_{\alpha-p}^{(n)} - \sum_{q \neq \alpha} \varepsilon_{\beta-q}^{(n)} \quad (5)$$

For the mixed-interstitial, the migration occurs through a series of translations and rotations, as described by Suzudo et. al [14]. To implement this process into the KMC model, we assume the mixed interstitial migrates via an initial

Table 1. Possible events within the SPPARKS KMC model. V=Vacancy, A,B = Atoms, AA = SIA, AB = Mixed Interstitial, S = Sink Site

	Vacancies	Interstitals	Instantaneous Processes	Deposition
KMC	V+A → A+V V+B → B+V	AA+A → A+AA AB+A → A+AB AB+B → B+AB AA ⟨111⟩ → AA⟨111⟩	AA+V → A+A AB+V → A+B AA+B → AB+A AA+S → A+S V+S → A+S AB+S → B+S	A → AA+V B → AB+V
SGMC	V+A → A+V V+B → B+V	AA+A → A+AA AB+A → A+AB AB+B → B+AB		A → B B → A

translation in the ⟨111⟩ direction, followed by a rotation and a second ⟨111⟩ translation. This results in an effective jump in the ⟨100⟩ direction relative to its original position, as shown schematically in figures 1 and 2. The change in energy for each translation in the process is calculated using equation 5 using the migration barrier for the mixed interstitial $E_m^{12} = 0.12\text{eV}$ [17]. For the rotation of the mixed interstitial dumbbell, a fixed activation energy, $E_R^{\text{MI}} = 0.03\text{eV}$, is used.

$$\Delta E_{i \rightarrow j}^{\text{MI}} = E_m^{\text{MI}} + \sum_p \varepsilon_{\alpha-p}^{(n)} - \sum_{q \neq \alpha} \varepsilon_{\beta-q}^{(n)} \quad (6)$$

To calculate the rate of this process we employ equation 8, where the time associated with a process, t^i , is given by $1/\lambda^i$

$$t_{\langle 100 \rangle}^{a \rightarrow d} = t_{\langle 111 \rangle}^{a \rightarrow b} + t_r^{b \rightarrow c} + t_{\langle 111 \rangle}^{c \rightarrow d} \quad (7)$$

$$\lambda_T = \frac{1}{1/\lambda_{\langle 100 \rangle}^{a \rightarrow c} + 1/\lambda_r + 1/\lambda_{\langle 111 \rangle}^{b \rightarrow c}} \quad (8)$$

2.2.2 Instantaneous Process and Deposition

Other events that occur within the KMC simulations are the recombination of defects, either with each other or at a sink, and the deposition of defects into the simulation box. When a vacancy and an interstitial come within third nearest neighbours (3NN) of each other, they recombine instantaneously leaving behind either two W atoms or a W and a Re atom depending on the interstitial type (W-W or W-Re respectively). When a defect comes within 3NN of a sink, it is also instantaneously recombined. For a vacancy this leaves behind a W atom, and for interstitials this results in either a W atom or a Re atom.

Because of the attractive binding energy between the SIA and a Re atom, we assume the transition of a SIA to a MI dumbbell to be instantaneous whenever a SIA comes within 3NN of a Re atom. The deposition of defects inserts a Frenkel pair into the simulation box. These

defects are inserted with a separation distance $2a$ where a is the lattice parameter. If the defects are within 3NN range, they are instantaneously recombined. This process occurs for a set deposition rate of N pairs per second. The inserted interstitial type depends on the site that is selected. A site is chosen at random within the box. If this site is a Re atom, a MI is inserted, and if it is a W a SIA is inserted, ensuring that solute concentration is conserved throughout the simulation.

3 Computational Results

3.1 SGMC

Figure 3 shows the equilibrated Re content as a function of the change in chemical potential, $\Delta\mu$. There is a clear jump in the concentration at lower temperatures indicating the presence of a miscibility gap. This implies that at 100 K there is a phase transformation predicted by this parameterisation.

As can be seen in figure 4, when point defects are introduced into the box clustering can occur. These simulations were carried out in a $2 \times 30 \times 30 \times 30$ atom box using a fixed defect concentration of 0.5% Vacancies and 0.1% Mixed interstitials respectively. The concentration of the vacancy simulation was 4%Re and 0.5%Re for the mixed interstitials. Both simulations were carried out at a fixed temperature of 600K. Mixed interstitials are strongly bound to each other as well as with Re and form clusters with Re attached. Interstitials can come together to form clusters because of their strong attractive binding, whereas the vacancies can cluster by forming an alternating structure with Re atoms. The vacancies only bind to each other very weakly and so do not have enough of an attraction to bind together on their own.

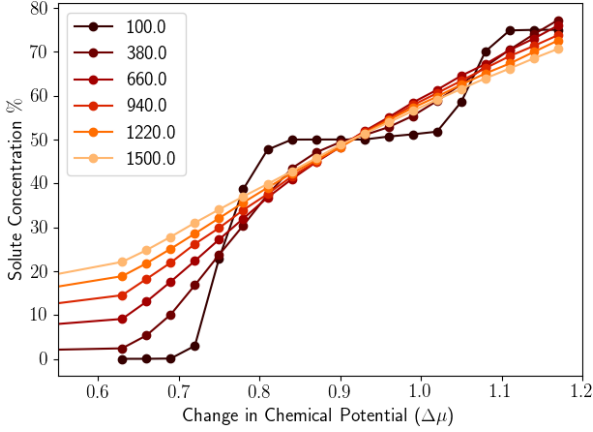


Fig. 3. Plot of equilibrated solute concentration in % as a function of the change in chemical potential $\Delta\mu$ for a range of temperatures.

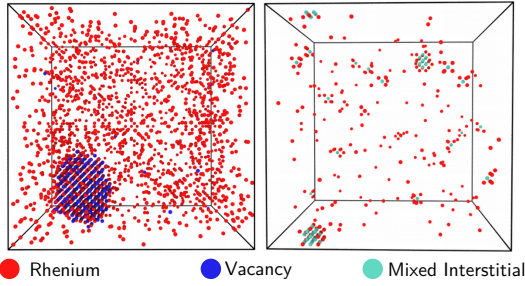


Fig. 4. Equilibrated configurations of W-Re-Vacancy and W-Re-Interstitial for a fixed starting defect concentration and change in chemical potential, $\Delta\mu$

3.2 Kinetic Monte Carlo

3.2.1 Calculation of Diffusion Coefficients

The diffusion coefficient for defects can be expressed as an Arrhenius-type equation as shown in equation 9, where E_A is the activation energy for migration, D_0 is the diffusion prefactor and T is the temperature.

$$D = D_0 \exp\left(-\frac{E_A}{kT}\right) \quad (9)$$

The diffusion of defects is affected by the presence of Re which slows down the migration. Local variations in the solute concentration can limit the migration of defects by trapping them. To quantify the effect that this has on the migration of defects within the model, the diffusion coefficient can be plotted as a function of Re concentration within the simulation box. The diffusion coefficient, D can also be given by equation 10:

$$\langle \Delta r^2 \rangle = 6D\Delta t \quad (10)$$

Table 2. Diffusion coefficient, D_0 and activation energy, E_A for vacancy diffusion as a function of solute concentration, x .

$x_{\text{Re}}(\%)$	D_0 (m^2s^{-1})	E_A (eV)
0.0	1.4×10^{-7}	1.64
0.5	2.61×10^{-7}	1.78
1.0	3.59×10^{-7}	1.84
5.0	2.56×10^{-7}	1.86

Table 3. Diffusion coefficient, D_0 and activation energy, E_A for solute diffusion as a function of solute concentration, x .

$x_{\text{Re}}(\%)$	D_0 (m^2s^{-1})	E_A (eV)
Self-diffusion Eq.9	6.49×10^{-7}	4.790
0.0	3.03×10^{-7}	4.79
5.0	2.20×10^{-7}	4.61
25.0	1.27×10^{-7}	4.08

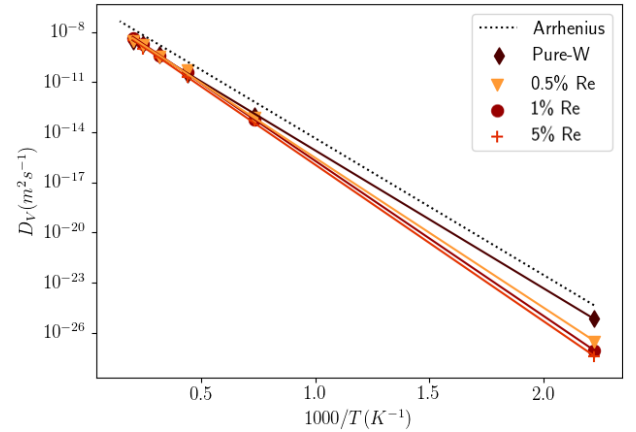


Fig. 5. Vacancy diffusivity, D_v , as a function of temperature and Re concentration. Dashed line shows the Arrhenius relationship described by equation 9.

where $\langle \Delta r^2 \rangle$ is the mean-squared-displacement and Δt is the time. To calculate the value of the diffusion coefficient, the trajectory of a defect or solute atom is output as a function of time. The trajectory is subdivided into different time steps, $\Delta t^{(i)}$ and the displacement that occurred during this timestep, $\Delta r^{(i)}$ is measured. The gradient of a linear fit of the square displacement vs time steps, $\Delta t^{(i)}$ divided by 6 gives the value of the diffusion coefficient.

The timestep in the KMC simulation, Δt_{kmc} is rescaled by the equilibrium vacancy concentration, C_{eq} , for simulations of solute diffusion. Typical vacancy concentrations are many orders of magnitude lower than can be simulated in a cell and so the timestep has to be rescaled for simulations of solute or self diffusion. The rescaled timestep, Δt , is given by equation 11.

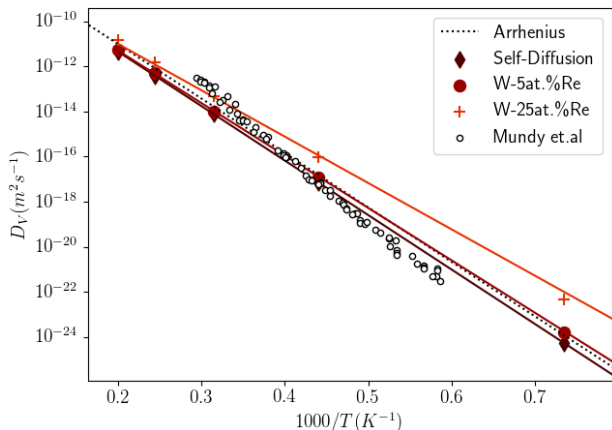


Fig. 6. Solute and self-diffusivity, D_s , as a function of temperature and Re concentration. Dashed line shows the Arrhenius relationship described by equation 9 using an activation energy of 4.79eV. The black points represent experimental values for the self-diffusion of W in W taken from [19]

$$\Delta t = \Delta t \frac{C}{C_{\text{eq}}} \quad (11)$$

The vacancy concentration in the simulation cell, C_{eq} is simply given by $1/N$ for simulations containing a single vacancy. The equilibrium vacancy concentration is calculated using equation 12 where the formation energy of the vacancy, E_F^V , is recalculated depending on the local environment.

$$C_{\text{eq}} = \exp\left(\frac{E_F^V}{kT}\right) \quad (12)$$

The instantaneous vacancy formation energy, E_F^V , is given by equation 13 and depends on the local environment of the defect.

$$E_F^V = -\frac{z_1}{2}\varepsilon^{(i)} - \frac{z_2}{2}\varepsilon^{(i)} + z_1\varepsilon^{(i)} + z_2\varepsilon^{(i)} \quad (13)$$

Figure 5 shows the vacancy diffusivity as a function of temperature and the solute concentration. Table 2 shows the diffusion coefficient, D_0 and the activation energy, E_A for each of the fitted lines. Figure 5 shows that the motion of the vacancies is slowed by the presence of Re in the simulation cell. Vacancies have an attractive binding to Re [17] and therefore are slowed by Re that they encounter in the box.

Figure 6 shows the average solute diffusivity, D_s as a function of temperature and solute concentration as well as the self-diffusion of W in W. The dashed line on figure 6 represents the Arrhenius relationship described by equation 9 using an activation energy of 4.79eV [17]. The dashed points represent experimental data points taken by J. N. Mundy et al. [19] for the self-diffusion of W. The diamond shaped markers represent the self diffusion calculated from our simulations. The other markers show the diffusivity of the solute atoms. The values for the solute

diffusivity are in good agreement with both the experimental data points and that predicted by equation 9. The introduction of 5%Re slightly decreases the solute migration activation energy as shown in table 3 which becomes more pronounced at 25%Re. This also agrees well with C. H. Huang et al's work using this parameterisation [17].

3.2.2 Radiation-induced segregation and Precipitation

As shown in figure 7, our model predicts the formation of a Re rich cluster around the point sink. This implies that there is a flux of defects towards this sink which transport Re to it, resulting in the formation of the cluster. We do not see the nucleation of a cluster without artificial sink introduction and Re clusters that are introduced are seen to dissolve back into solute without the presence of a sink. The mechanism proposed by C. H. Huang et al suggests that the immobilisation of the mixed interstitials by Re or by other mixed interstitials provides the vacancy sufficient time to migrate to the trapped dumbbell and recombine. This means that the trapped interstitial effectively acts as the sink that we have introduced artificially. However, using our model we observe that the interstitial when it reaches a Re rich zone, first becomes trapped in that zone as suggested, but then continues to dissolve the cluster over time. In the time it takes the vacancy to reach the immobilised interstitial, it has time to dissolve the cluster slightly, reducing the Re content and reducing the effectiveness of the cluster to trap further interstitials. Over many of these events the cluster reaches a point at which it is too diffuse to act as a trapping site and it is dissolved back into the matrix.

Figure 8 shows the Re concentration in the cluster as a function of radius from the point sink. The concentration is estimated in a series of progressively smaller concentric spherical shells. As seen in figure 8 when a sink is artificially introduced into the box, there is strong Re segregation to the sink. After 100s of irradiation the maximum concentration of Re at the sink is between 25 and 30 at.%. This agrees well with experimental data from A. Xu et al's ion implantation which shows a maximum cluster concentration of around 30at.% [6]. We do not see the saturation of the Re content at 50% in the centre of the precipitate but overall it is lower than the level predicted by C. H. Huang et al [17]. This could be due in part to the increased cluster dissolution that we see in our model.

There is competition between the transport of Re to the sink and the thermodynamic driving force for dissolution. Without a flux of defects to the sink, our model predicts the dissolution of the Re cluster back into solution, in agreement with the phase diagram. This would imply that if an irradiated W-Re sample were to be annealed, the clusters would dissolve back into solution. This means that in order to facilitate cluster growth there needs to be a continuous flux of Re towards a sink. Both the mixed interstitials and the vacancies bind to Re and therefore drag it towards the sink. The mixed interstitial is also comprised of two atoms, one of which is a Re, so just by moving to the sink it transports Re to it, and very rapidly

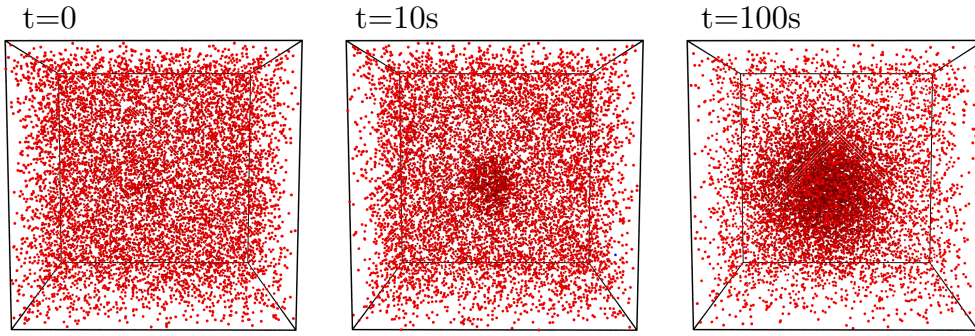


Fig. 7. Precipitation of Re around a point sink at 10 and 100s of irradiation in a W-2at.%Re alloy. A dose rate of $1e-3$ dpa/s was used at an irradiation temperature of 1800K which ensures that vacancies are mobile within our simulation

due to its 3D motion and low activation energy for migration. In order to facilitate the nucleation of clusters without the introduction of a sink it might therefore be necessary to use a much higher dose so that the probability of two mixed interstitials binding is increased.

Figure 9 shows the growth of the cluster shown in figure 7 as a function of time. A cluster is defined as the region within which the Re concentration is above 5% which we approximate as spherical. Plotted in figure 9 is the radius beyond which the concentration drops below 5% as a function of the irradiation time in seconds. We see the continuous growth of the cluster from the moment the sink is introduced at time $t=0$. As time progresses up to 100s, there is a slight decrease in the growth rate as more Re from the bulk is contained within the cluster. Overall the growth of the cluster is slower than observed by C. H. Huang et al. but begins to approach a similar size after 100s. In C. H. Huang et al simulations the cluster reaches its maximum size of around 4nm after only 20-30s. In our simulations the cluster reaches 4nm after around 40-50s but does not stop growing at that point. The growth after this point is reached is slowed but still progresses. This could be due to the fact that the Re concentration in the cluster doesn't increase as rapidly in our simulations, as shown in figure 8 where the central concentration reaches only 30% after 100s compared to 50% in C. H. Huang et al simulations. Compared to A. Xu et al's experiments we see a similarly sized Re clusters to the ion implantations conducted at 773K [6].

3.2.3 Grain Boundary Segregation

The segregation of Re to grain boundaries (GB) in tungsten alloys has been observed experimentally and computationally. The decoration of grain boundaries with Re has the potential to create localised embrittlement and premature failure through the degradation of fracture toughness. Klimnkov et al. saw GB decoration with Re and Os from transmutation in neutron irradiated W, with a post irradiation composition of W-1.4Re-0.1Os [9].

To study the decoration of GBs using our model, we introduce a planar point-defect sink to represent the GB. If a defect comes within the recombination range (3NN)

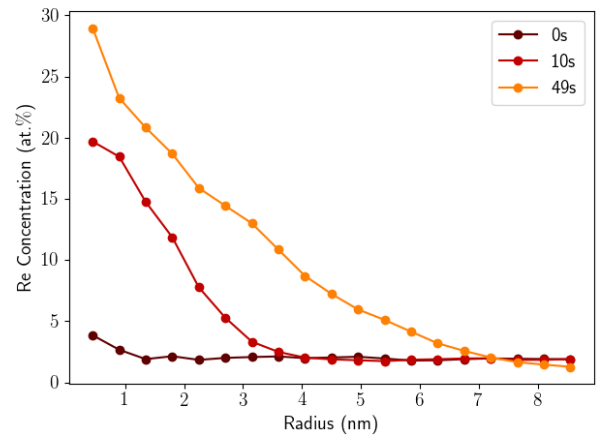


Fig. 8. Segregation of Re in a 1.4at.%Re allot to a planar ideal sink at 1800K after a total dose of 5.83dpa with a dose rate of 1.19dpa/s.

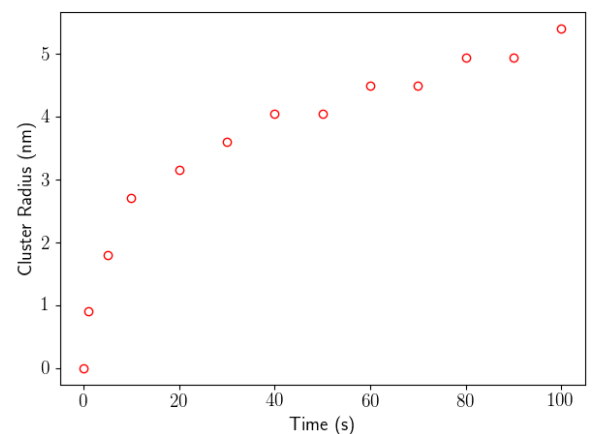


Fig. 9. Growth of cluster in terms of the number of atoms in the cluster as a function of irradiation time for the simulation shown in figure 7

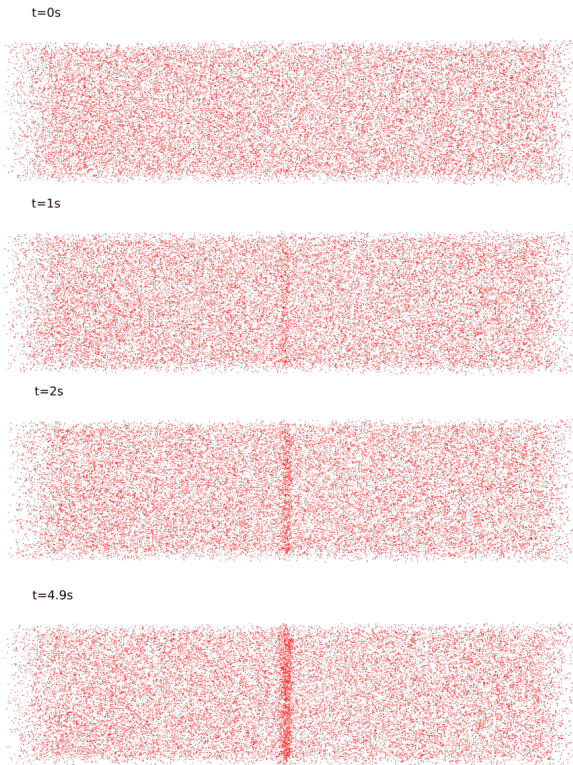


Fig. 10. Segregation of Re in a 1.4at.%Re allot to a planar ideal sink at 1800K after a total dose of 5.96×10^{-3} dpa with a dose rate of 1.19×10^{-3} dpa/s.

of this 2d plane it is removed instantaneously. There is no crystallographic difference between the cell on either side of the planar sink. We place this sink in the centre of a $2 \times 64 \times 64 \times 256$ atom box of W-1.4at.%Re and insert defects at a rate of 1.19×10^{-3} dpa/s at a temperature of 1800K.

Figure 10 shows the Re atoms in the simulation cell. There is a clear segregation of Re to the GB in the centre of the box. After 5 s of exposure the GB in the simulation cell had accumulated Re up to a maximum concentration of approximately 8 at.%Re. The simulation was carried out at 1800 K, which is significantly higher than most ion irradiation experiments can achieve (typically around 1200 K). This temperature was used to accelerate the motion of defects, in particular diffuse much more slowly at 1200K. The results shown in figure 10 are discussed in comparison to experimental data in section 4.3

4 Experimental Results

As discussed previously there are currently no facilities that are capable of exposing candidate materials to fission spectrum neutrons at sufficiently high temperatures

and doses to directly study the degradation of plasma facing components. Analysis of candidate materials is typically conducted using either ion irradiation or fission spectrum neutron irradiation. Charged particles such as ion deposit their energy over a much shorter range than neutrons and so induce damage in a shallow damaged layer on the surface of the material. Fission neutron irradiation is the closest means of reproducing the damage but typically exposes the material to a different energy spectrum resulting in a different post irradiation concentration. By alloying samples with compositions following the predicted transmutation pathway, the behaviour of these elements may be studied more systematically. In this section we study 2 ion implanted samples using Atom Probe Tomography (APT), a W-1.4at.%Re and a W-25at.%Re sample. The W-1.4at.%Re sample was fabricated in order to match the post irradiation composition of the neutron irradiated W sample from the Extremat II program, studied using STEM-High Angle Annular Dark Field Imaging and Atom Probe Tomography [9, 13].

4.1 Ion Implantation

Ion implantation was used to introduce point defects into model W-Re alloys. W-1.4Re and W-25Re samples were produced by arc melting. They were prepared for implantation by grindings and polishing with a series of successively finer grit SiC grinding papers, diamond suspension and colloidal silica.

Two sets of ion implantations were carried out: the W-1.4Re was carried out at the Joint Accelerators for Nano-Science and Nuclear Simulation (JANNuS) facility at CEA Saclay. The samples were implanted with W^{9+} ions accelerated to 24MeV at a temperature of 1073K. Aluminium degrader foils of 0.8, 2 and 3 μm were used to flatten the irradiation profile to produce a more uniform distribution of dpa through the material. The average ion flux was $7.0 \times 10^{14} \text{m}^{-2} \text{s}^{-1}$ for 11580s. The W-25Re sample was implanted at the Surrey Ion Beam Centre as part of an earlier series of implantations carried out by Alan Xu et. al [6, 7]. The sample was implanted to a total of 33dpa at 773K using 2MeV W ions. No degrader foils were used to flatten the profile in the W-25%Re samples.

4.2 Atom Probe Tomography

Samples were prepared for Atom Probe Tomography (APT) using the Focused Ion Beam (FIB) liftout technique using a Zeiss NVision 40 dual beam FIB-SEM. A protective region (15 $\mu\text{m} \times 1.5\mu\text{m}$) of C was deposited on the surface of the samples using a Gas Injection System (GIS), and for site specific liftouts was aligned along a grain boundary. The region was undercut using a beam current of 1.5nA and an accelerating voltage of 30kV. The cantilever was lifted out and mounted onto a 22 post silicon coupon, and sharpened into a tip roughly 100nm in diameter using an annular milling pattern and a series of successively smaller radii and beam currents between 1.5nA - 40pA at 30kV.

Once sharpened, the tips received a final polishing stage at 2kV, 300pA to remove Ga implanted material from the FIB beam, removing approximately 50-100nm of material.

APT was carried out in laser mode in a CAMECA[®] LEAP 5000 XR using a sample temperature of 55K, a laser pulse energy of 125pJ and a pulse frequency of 100kHz. The data was reconstructed and visualised using IVAS[®] 3.8.4. The laser energy was run at a high energy in order to maximise sample yield without degrading the quality of the mass spectrum due to peak broadening.

4.3 Grain Boundaries

APT of the sample showed bulk clustering of Re away from the grain boundaries. However, the clusters were less pronounced than in previous studies by A. Xu et al. where spherical precipitates were observed. In these samples we observe that the clusters produced are more diffuse in nature. Figure 11 shows a reconstruction of the data containing a grain boundary in the W-1.4at.%Re sample. The grain boundary is decorated with Re and has a region around it approximately 20nm across. On either side of the grain boundary are regions which appear similar to bulk regions of the same sample. Diffuse regions of increased Re content are observed.

Figure ?? shows the decoration of the grain boundary in the APT compared to that observed in the KMC simulation shown in figure 10. For the APT the depletion of the region around the GB is seen on either side of the central peak. The peak Re concentration at the GB is between 4-5at.%Re. For the KMC simulation there is a higher concentration at the GB despite the fact that a lower dose has been used. The temperature of the simulation was 1800K in order to increase the mobility of the defects which may have accelerated the diffusion of defects and therefore Re to the GB.

4.4 Re Precipitation

We also analysed a W-25Re ion implanted sample. The majority of work on ion implanted W-Re shows that roughly spherical precipitates are formed, however, many studies of neutron irradiated W where the Re has been introduced through transmutation show that rod shaped precipitates can be formed. Figure 13 shows the reconstruction of the W-25Re sample.

In the W25Re sample, rod shaped precipitates were seen, with a size varying with implantation depth, as shown in figure 13. Under neutron irradiation, particularly when the Re content is high, several studies have shown the formation of rod/needle shaped Re rich precipitates which are associated with chi or sigma phase formation [12,20]. Under ion irradiation, samples with lower Re content typically tend to form clusters roughly spherical in shape that are thought to be a precursor to precipitation [6,7]. The size and shape of the clusters appears to vary with implantation depth, with smaller clusters being observed nearer to the surface of the sample.

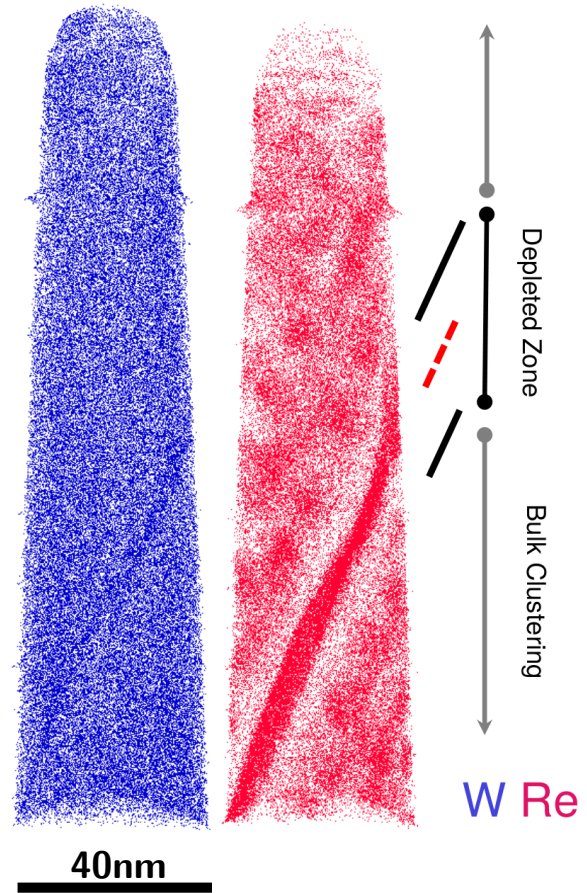


Fig. 11. APT reconstruction of W-1.4Re sample ion irradiated to 1.67dpa at 1073K. Re atoms shown in Red, all other atoms hidden. Grain boundary visible decorated with Re surrounded by a region depleted in Re compared to the bulk

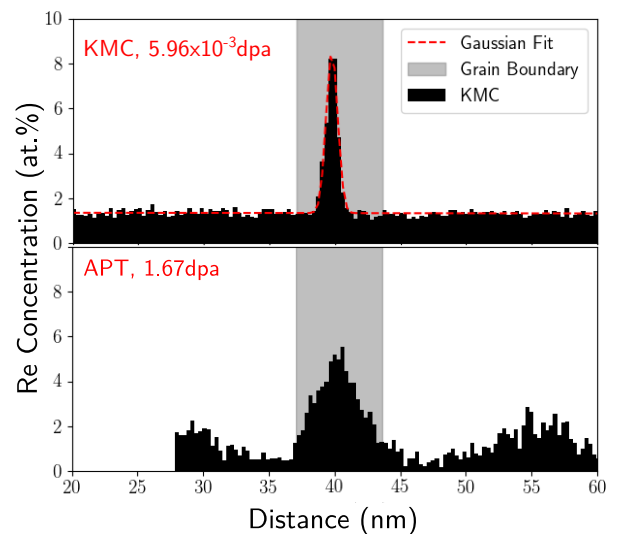


Fig. 12. Segregation of Re in a 1.4at.%Re allot to a planar ideal sink at 1800K after a total dose of 5.83dpa with a dose rate of 1.19dpa/s.

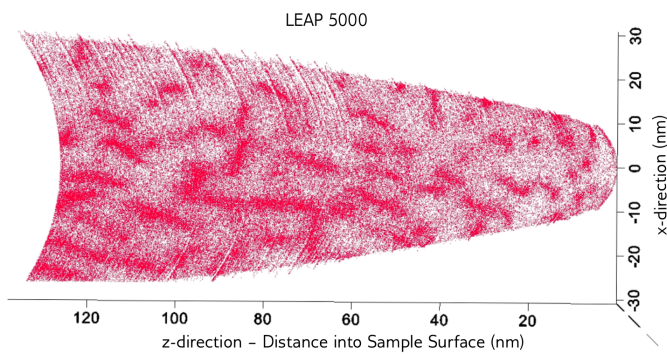


Fig. 13. APT reconstruction of W-25Re sample ion irradiated to 33dpa at 773K. Re atoms shown in Red, all other atoms hidden

5 Conclusions

In this research, a Monte Carlo model, implemented into the open source code, SPPARKS, based on pairwise interactions constructed using the broken-bond model and parameterised using values from DFT calculations is presented. Kinetic Monte Carlo simulations show the segregation of Re to sinks and the formation of clusters that have previously been observed experimentally. We see a central cluster concentration of 29at.%Re in a W-2at.%Re alloy after 100s at of irradiation with a dose rate of 1×10^{-3} dpa/s at temperature of 1800K, resulting in a total dose of 0.1dpa. Though the conditions are different, this is similar to the concentration observed experimentally for similar alloy compositions. We also see the decoration of a simulated grain boundary with Re, that we model as a planar ideal sink. We present a preliminary comparison to APT data of a GB in ion implanted w-1.4at.%Re, irradiated to 1.67dpa at 1073K. Though we see the decoration of the GB both experimentally and computationally, there are key differences which are most likely a result of the different irradiation conditions used.

6 Acknowledgements

Funding: M.J.L.'s work was supported by the UK Engineering and Physical Sciences Research Council [EP/N509711/1] and the Culham Centre for Fusion Energy (CCFE), United Kingdom Atomic Energy Authority through an Industrial CASE scholarship, [Project Reference Number 1802461]. Atom Probe Tomography was carried out at the Oxford Materials Atom Probe Group. The CCFE work has been carried out within the framework of the EUROfusion Consortium and has received the funding from Euratom and training programme 2014-2018 under grant agreement No. 633053 and from the RCUK Energy Programme [grant number EP/P012450/1]. The views and opinions expressed herein do not necessarily reflect those of the European Commission. M.J.L would also like to thank Alan Xu for preparing the W-25Re sample that was used in this study. E.M. acknowledges support by the U.S. Department of Energy, Office of Science, Office of Fusion Energy

Sciences, and Office of Advanced Scientific Computing Research through the Scientific Discovery through Advanced Computing (SciDAC) project on Plasma-Surface Interactions under award number DE-SC0008875.

References

1. M. Rieth *et al.*, "Recent progress in research on tungsten for nuclear fusion applications in europe," *Journal of Nuclear Materials*, vol. 432, no. 1-3, pp. 482–500, 2013.
2. D. Armstrong, P. Edmondson, and S. Roberts, "Effects of sequential tungsten and helium ion implantation on nano-indentation hardness of tungsten," *Applied Physics Letters*, vol. 102, no. 25, p. 251901, 2013.
3. R. Abernethy, "Predicting the performance of tungsten in a fusion environment: a literature review," *Materials Science and Technology*, vol. 33, no. 4, pp. 388–399, 2017.
4. M. Gilbert and J.-C. Sublet, "Neutron-induced transmutation effects in w and w-alloys in a fusion environment," *Nuclear Fusion*, vol. 51, no. 4, p. 043005, 2011.
5. M. Gilbert, J.-C. Sublet, and S. Dudarev, "Spatial heterogeneity of tungsten transmutation in a fusion device," *Nuclear Fusion*, vol. 57, no. 4, p. 044002, 2017.
6. A. Xu, C. Beck, D. E. Armstrong, K. Rajan, G. D. Smith, P. A. Bagot, and S. G. Roberts, "Ion-irradiation-induced clustering in w-re and w-re-os alloys: A comparative study using atom probe tomography and nanoindentation measurements," *Acta Materialia*, vol. 87, pp. 121–127, 2015.
7. A. Xu, D. E. Armstrong, C. Beck, M. P. Moody, G. D. Smith, P. A. Bagot, and S. G. Roberts, "Ion-irradiation induced clustering in w-re-ta, w-re and w-ta alloys: An atom probe tomography and nanoindentation study," *Acta Materialia*, vol. 124, pp. 71–78, 2017.
8. S. Maloy, M. James, W. Sommer Jr, G. Willcutt Jr, M. Lopez, T. Romero, and M. B. Toloczko, "The effect of 800 mev proton irradiation on the mechanical properties of tungsten at room temperature and at 475 c," *Journal of Nuclear Materials*, vol. 343, no. 1-3, pp. 219–226, 2005.
9. M. Klimenkov, U. Jäntschi, M. Rieth, H. Schneider, D. Armstrong, J. Gibson, and S. Roberts, "Effect of neutron irradiation on the microstructure of tungsten," *Nuclear Materials and Energy*, vol. 9, pp. 480–483, 2016.
10. A. Hasegawa, M. Fukuda, S. Nogami, and K. Yabuuchi, "Neutron irradiation effects on tungsten materials," *Fusion Engineering and Design*, vol. 89, no. 7-8, pp. 1568–1572, 2014.
11. Y. Katoh, L. Snead, L. Garrison, X. Hu, T. Koyanagi, C. Parish, P. Edmondson, M. Fukuda, T. Hwang, T. Tanaka, *et al.*, "Response of unalloyed tungsten to mixed spectrum neutrons," *Journal of Nuclear Materials*, 2019.
12. X. Hu, C. M. Parish, K. Wang, T. Koyanagi, B. P. Eftink, and Y. Katoh, "Transmutation-induced precipitation in tungsten irradiated with a mixed energy neutron spectrum," *Acta Materialia*, vol. 165, pp. 51–61, 2019.
13. M. J. Lloyd, R. G. Abernethy, M. R. Gilbert, I. Griffiths, P. A. J. Bagot, M. P. Moody, and D. E. J. Armstrong, "Decoration of voids with rhenium and osmium transmutation products in neutron irradiated single crystal tungsten," submitted to *Scripta Materialia*, 2019.

14. T. Suzudo, M. Yamaguchi, and A. Hasegawa, "Stability and mobility of rhenium and osmium in tungsten: first principles study," *Modelling and Simulation in Materials Science and Engineering*, vol. 22, no. 7, p. 075006, 2014.
15. T. Suzudo, M. Yamaguchi, and A. Hasegawa, "Migration of rhenium and osmium interstitials in tungsten," *Journal of Nuclear Materials*, vol. 467, pp. 418–423, 2015.
16. T. Suzudo and A. Hasegawa, "Suppression of radiation-induced point defects by rhenium and osmium interstitials in tungsten," *Scientific reports*, vol. 6, p. 36738, 2016.
17. C.-H. Huang, L. Gharaee, Y. Zhao, P. Erhart, and J. Marian, "Mechanism of nucleation and incipient growth of re clusters in irradiated w-re alloys from kinetic monte carlo simulations," *Physical Review B*, vol. 96, no. 9, p. 094108, 2017.
18. J. Wróbel, D. Nguyen-Manh, K. Kurzydłowski, and S. Dudarev, "A first-principles model for anomalous segregation in dilute ternary tungsten-rhenium-vacancy alloys," *Journal of Physics: Condensed Matter*, vol. 29, no. 14, p. 145403, 2017.
19. J. Mundy, S. Rothman, N. Lam, H. Hoff, and L. Nowicki, "Self-diffusion in tungsten," *Physical Review B*, vol. 18, no. 12, p. 6566, 1978.
20. A. Hasegawa, M. Fukuda, K. Yabuuchi, and S. Nogami, "Neutron irradiation effects on the microstructural development of tungsten and tungsten alloys," *Journal of Nuclear Materials*, vol. 471, pp. 175–183, 2016.